Reduction of Hydrogenated ZrO$_2$ Nanoparticles by Water Desorption

Antonio Ruiz Puigdollers,[†] Francesc Illas,[‡] and Gianfranco Pacchioni*,[†]

[†]Dipartimento di Scienza dei Materiali, Università Milano—Bicocca, Via R. Cozzi 55, 20125 Milan, Italy

[‡]Departament de Ciència de Materials i Química Física and Institut de Química Teòrica i Computacional (IQTCUB), Universitat de Barcelona, 08028 Barcelona, Spain

ABSTRACT: Reduction of zirconia by water desorption from a hydrogenated surface is the topic of this study. The focus is on the role of nanostructuring the oxide reducibility measured by the cost of formation of oxygen vacancies by water desorption. We have performed density functional theory calculations using the Perdew−Burke−Ernzerhof + U approach and including dispersion forces on the adsorption, dissociation, diffusion of hydrogen on the ZrO$_2$ (101) surface and on Zr$_{16}$O$_{32}$, Zr$_{40}$O$_{80}$, and Zr$_{80}$O$_{160}$ nanoparticles (NPs). The process involves the formation of a precursor state via diffusion of hydrogen on the surface of zirconia. The results show that O vacancy formation via H$_2$O desorption is more convenient than via direct O$_2$ desorption. The formation of an O$_s$H$_2$ surface precursor state to water desorption is the rate-determining step. This step is highly unfavorable on the ZrO$_2$ (101) surface both thermodynamically and kinetically. On the contrary, on zirconia NPs, characterized by the presence of low coordinated ions, water desorption becomes accessible such that even at temperatures close to 450 K the reaction becomes exergonic. The study shows the role of nanostructuring on the chemical and electronic properties of an oxide.
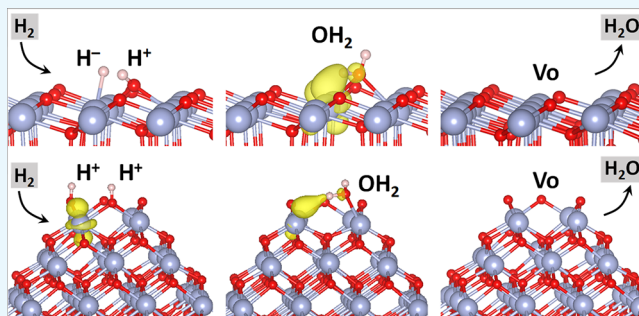
1. INTRODUCTION

Metal oxides represent a very wide class of heterogeneous catalysts. They can behave as inert supports for an active metal particle or can directly participate in the catalytic process via active surface species and/or basic/acid sites. The composition, structure, and size of the oxide catalyst determine its chemical activity. Zirconium dioxide (ZrO$_2$) has been extensively used in various catalytic processes. For example, in reactions involving hydrogen, zirconia is used in hydrogenation reactions of CO$_2$ and CO to synthesize organic molecules,[1−3] as well as in solid oxide fuel cells for the electrochemical oxidation of H$_2$ thanks to its stability over a wide range of oxygen pressure and mechanical strength.[4] In another context, zirconia is used as a catalyst for ketonization reactions in the upgrading of bio-oil to reduce the oxygen content of the biomass after a pyrolysis treatment.[5,6]

ZrO$_2$ is considered to be a nonreducible oxide, more similar to MgO and SiO$_2$ than to TiO$_2$ or CeO$_2$. This can be attributed to the high ionicity and wide band gap of ZrO$_2$.[7,8] This is a property observed in large crystallites of zirconia, generally referred to as bulk zirconia. The nonreducible nature of zirconia emerges quite clearly when the material is exposed to hydrogen. The H$_2$ molecule adsorbs and dissociates on extended zirconia surfaces through a heterolytic mechanism in which OH$^+$ and ZrH$^-$ surface groups are formed. This means that no oxide reduction takes place (no formation of adsorbed protons and of Zr^{3+} ions).[9−11] Another indicator of the low reducibility of this oxide comes from the cost to create a surface O vacancy in the bulk or on the surface of the material (∼6 eV[12]). However, the

physical and chemical properties of oxides can change dramatically when the material is prepared in the form of nanoparticles (NPs), nanowires, and thin films or in general is nanostructured.[13,14] In fact, quantum confinement effects, undercoordination, and the special structural flexibility typical of many nanostructures, often referred to as fluxionality, result in novel properties that are not observed in the bulk regime.[15−17] For instance, we have recently found that zirconia prepared in the form of 1−2 nm particles splits the H$_2$ molecule through a homolytic process, with the formation of Zr^{3+} (4d^1) centers. This is the same mechanism observed on reducible oxides such as TiO$_2$ and CeO$_2$.[18−20] In this process, two OH$^+$ species form and two electrons (coming from the H$_2$ molecule) reduce two low coordinated Zr^{4+} to Zr^{3+} centers (giving rise to a magnetic ground state).[8,21] In addition, the formation energy of a neutral O vacancy decreases by 2−3 eV when it is created on special sites of the NP.[7,8] The reducible character of the nanostructures comes from the presence of low coordinated Zr sites in edges and corners, which introduce low-lying Zr 4d states that accept the charge released from the H$_2$ molecule or from the removed O atom.

In general, the interest toward novel forms of reduced ZrO$_2$ is increasing. For example, it has been demonstrated that O-deficient ZrO$_{2−x}$ NPs display better catalytic activity in reactions of transformation of biomass into fuels,[5,22,23] high-

temperature hydrocarbon conversion,[24] and H_2 production under solar light, all reactions where stoichiometric ZrO_2 is less active or even inert.[25] The enhanced catalytic activity has been related to the presence of surface acidic Zr^{3+} sites. In a different field, reduced, dopant-free ZrO_2 nanostructures have been shown to exhibit ferromagnetic behavior because of the presence of oxygen vacancies.[26]

Apart from direct interaction with H_2, there are several mechanisms for the reduction of the oxide surface. In the presence of deposited metal particles, O surface ions can spill over the metal, leaving a surface O vacancy (reverse spillover). This process has been estimated to cost only 0.2 and 0.6 eV on a Ru_{10} cluster supported on TiO_2 and ZrO_2, respectively.[27] The cost is expected to be even lower at surface steps and edges[28,29] and is further reduced when the metallic clusters are supported on an oxide NP.[30] The oxide surface can also be reduced by a hydrogenation process and subsequent desorption of water, leaving behind an O vacancy and its associated charge (H_2 + $O^{2-} \rightarrow H_2O + 2e^-_{(Vo)}$). In the latter case, the presence of a supported metal particle can facilitate the dissociation of H_2 and the spillover of hydrogen on the surface to form OH^+ groups and reduced metal cations. Alternatively, O surface ions can spill over the metal particle and react with the adsorbed H atoms to form H_2O, leaving behind an O vacancy.[31−33]

In the absence of supported metal particles, the direct reduction process $ZrO_2 + H_2 \rightarrow ZrO_{2-x} + H_2O$ is highly endothermic for extended zirconia surfaces because of the low reactivity toward H_2 and the high cost to create an O vacancy (~6 eV[12]). Hofmann et al. found an enthalpy of +2.71 eV for the reduction reaction on the (101) surface of tetragonal zirconia from density functional theory (DFT) Perdew−Burke−Ernzerhof (PBE) calculations.[34] A higher value, +3.57 eV, has been found by our group using the PBE + U approach that improves the description of the zirconia band gap. The process involves an energy barrier of 2.55 eV.[35] The large enthalpy and energy barrier explain the experimental observation that H_2 desorption instead of H_2O desorption takes place from the ZrO_2 surface when the hydroxylated Ru/ZrO_2 system is heated to 370 K.[36] This study follows other studies from our group on the topic of zirconia NPs and related properties. We first analyzed the general features and the electronic structure of zirconia NPs of different sizes, elucidating the role of low coordinated ions and the corresponding presence of new defect states in the band gap of the material.[7,8] In this work, we also considered the cost of formation of oxygen vacancies via O_2 desorption, as this is a possible route to generate reduced samples. In a subsequent study, we have considered metal adsorption on the ZrO_2 NP, in particular, the interaction of Au atoms and their ability to exchange charge with the oxide support as a function of the particle size.[37] In a third study, we considered H_2 adsorption and dissociation, showing that zirconia NPs behave in a completely different way compared to bulk zirconia as far as interaction with hydrogen is concerned.[21] In the present study, the work has been extended toward another important topic: the formation and desorption of water from hydrogenated ZrO_2 NPs. In particular, we have investigated two steps of the reduction process on zirconia NPs from both thermodynamic and kinetic points of view. First, the H_2 molecule is dissociated on the NP surface (step I). Second, one H atom diffuses into the OH group to form the O_sH_2 surface complex that is then desorbed as H_2O (step II).

I—hydrogenation $ZrO_2 + H_2 \rightarrow H_2ZrO_2$

II—dehydration $H_2ZrO_2 \rightarrow ZrO_{2-x} + H_2O$

In addition, we have investigated the barriers for diffusion of the H atoms into distant adsorption sites, a process that contrast the formation of an O_sH_2 surface complex. In general, water desorption from a hydroxylated oxide surface is a viable mechanism, leading to the reduction of an oxide. The present work shows the relevant role of nanostructuring in favoring the process that can result in substantial differences in the chemical behavior of the same material when prepared in a bulk form or in the form of nanostructures.

2. COMPUTATIONAL DETAILS

DFT-based calculations were performed with the Vienna Ab-Initio Simulation Package (VASP 5.3),[38,39] with plane waves as basis sets with a kinetic energy cutoff of 400 eV. The PBE exchange−correlation functional, within the generalized gradient approximation (GGA), was applied.[40] The GGA + U approach implemented by Dudarev et al.[41,42] was used to partly correct the self-interaction error intrinsic in GGA functionals. An on-site Coulomb correction, $U_{eff} = U - J$, was set to 4 eV for the 4d states of Zr atoms. This value provided lattice parameters for tetragonal ZrO_2: a_0 = 3.662 Å and c_0 = 5.223 Å, in good agreement with the experimental ones, 3.64 and 5.27 Å, respectively.[43] The calculated Kohn−Sham band gap, 4.5 eV, is still considerably smaller than the experimental value 5.78 eV.[44] The DFT + U approach is not free from limitations and should be considered as a pragmatic way to partly remove the self-interaction error inherent to DFT. Furthermore, U values depend on coordination and might change during the transition-state search. In this respect, the results presented in the following must be considered as qualitative rather than quantitative. However, the main purpose of this work is to compare, using the same approach, the properties of zirconia in an extended or a nanostructured form. In this respect, because some of the energies discussed for the two set of systems differ substantially, the results and the general conclusions are not expected to depend on the choice of the U parameter.

Long-range dispersion forces are included by means of the D2' method[45] on top of the PBE functional; this is a slight modification of the original parametrization of the D2 approach proposed by Grimme[46] in which we changed the parameters C_6 and R_0 of the DFT-D2 approach, as suggested by Tosoni and Sauer.[47]

The (101) surface of tetragonal ZrO_2 was modeled with a five-layer 3 × 2 supercell containing a total of 180 atoms ($Zr_{60}O_{120}$). The lattice parameters were fixed at the bulk t-ZrO_2 optimized structure obtained with a plane-wave basis set with a kinetic energy of up to 600 eV and with an 8 × 8 × 8 Monkhorst−Pack k-point grid. We modeled octahedral-based zirconia NPs with compositions $Zr_{16}O_{32}$, $Zr_{40}O_{80}$, and $Zr_{80}O_{160}$ having diameters of 0.9, 1.5, and 1.9 nm, respectively.[7,8] The models were cut from bulk tetragonal ZrO_2, exhibiting {101} surfaces in the octahedral facets and {100} surfaces in the cut corners, which are the two most stable surfaces for this phase. The geometry optimizations of both slab and NPs were carried out at the Γ-point, up to ionic forces smaller than |0.05| eV/Å and a threshold of 10^{-5} eV for the electronic self-consistent cycles.

The reaction energy for the hydrogenation (step I) and water desorption (step II) has been calculated according to

$$\Delta E_I = E(H_2ZrO_2) - E(ZrO_2) - 1/2E(H_{2,(g)}) \qquad (1)$$

$$\Delta E_{II} = E(ZrO_{2-x}) + E(H_2O_{(g)}) - E(H_2ZrO_2) \qquad (2)$$

where $E(H_2ZrO_2)$ is the energy of the hydrogenated zirconia, $E(ZrO_2)$ is the energy of clean zirconia, $E(ZrO_{2-x})$ is the energy of zirconia with one O vacancy, and $E(H_{2,(g)})$ and $E(H_2O_{(g)})$ are the energies of H_2 and H_2O molecules in the gas phase, respectively. The same equations are used to calculate the reaction Gibbs free energy, ΔG, of the reaction steps. The free energies $G(ZrO_2)$ and $G(ZrO_{2-x})$ are approximated to the PBE + U energy, and those for H_2, H_2O, and H_2ZrO_2 are defined according to

$$G(H_{2,(g)}, \; H_2O_{(g)}) \approx E_{PBE} + ZPE - T \cdot S \qquad (3)$$

$$G(H_2ZrO_2) \approx E_{PBE} + ZPE \qquad (4)$$

where ZPE is the zero-point energy calculated as $(\Sigma h\nu_i)/2$, for which only O–H and Zr–H vibrations (ν) are considered, T is the temperature, and S is the total entropy. In the $G(H_2ZrO_2)$ term, the vibrational internal energy, U_{vib}, and the vibrational entropy, S_{vib}, have been neglected. This is justified because OH and ZrH vibrations, in the range of 3000–3700 and 1400 cm^{-1}, respectively, yield U_{vib} and S_{vib} terms on the order of 10^{-6} eV only. The entropy of H_2 and H_2O molecules in the gas phase is calculated as the sum of the translational, S_{trans}, vibrational, S_{vib}, and rotational, S_{rot}, contributions according to eqs 5–7

$$S_{trans} = k_B \left(\frac{5}{2} + \ln q_{trans} \right) \qquad (5)$$

$$S_{vib} = k_B \left[\frac{\theta/T}{e^{\theta/T} - 1} - \ln(1 - e^{-\theta/T}) \right] \qquad (6)$$

$$S_{rot} = k_B \left[1 + \ln\left(\frac{IT}{\sigma}\right) + \ln\left(\frac{8\pi^2 k_B}{h^2}\right) \right] \qquad (7)$$

where q is the partition function, θ is the vibrational temperature ($h\nu/k_B$), and I is the inertia moment. At 298 K and 1 bar, our calculated entropies for H_2 and H_2O, 131 and 189 J/mol·K, respectively, perfectly agree with those reported in the literature.[48]

Finally, transition states are computed by means of the nudged elastic band method using the climbing image approach[49] and fully characterized by pertinent vibrational analysis.

3. RESULTS AND DISCUSSION

3.1. Thermodynamics of Hydrogenation and Dehydration of ZrO$_2$ NPs.
The first step of the reduction process investigated is the adsorption and dissociation of a H_2 molecule on the zirconia surface (hydrogenation). As mentioned above, bulk ZrO$_2$ and ZrO$_2$ (101) surface are nonreducible. The regular (101) surface dissociates the H_2 molecule through a heterolytic mechanism into H$^+$ and H$^-$ ions, Figure 1a, with a slightly exothermic process, −0.06 eV, Table 1. The Gibbs free energy for the dissociation is endergonic at 298 K and 1 bar, with $\Delta G_I = +0.34$ eV, because of the entropy of H_2 gas that hinders the adsorption and dissociation.

A completely different situation is obtained on NPs. An important aspect to consider in the study of ZrO$_2$ NPs is how the chosen structures are representative of real NPs. First of all, we decided to consider three stoichiometric particles of
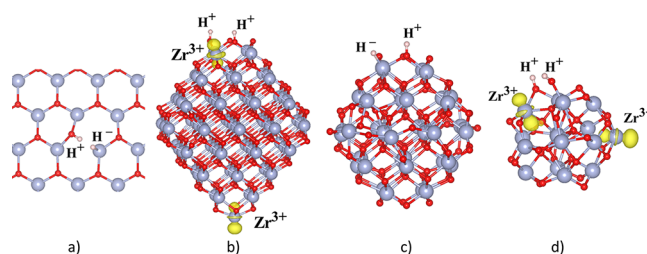
Figure 1. Structures of hydrogenated zirconia: (a) ZrO$_2$ (101) surface; (b) Zr$_{80}$O$_{160}$, (c) Zr$_{40}$O$_{80}$, and (d) Zr$_{16}$O$_{32}$ NPs. Zr: blue atoms; O: red atoms; and H: white atoms. The reduction of two Zr^{4+} to Zr^{3+} in Zr$_{80}$O$_{160}$ and Zr$_{16}$O$_{32}$ is clearly seen from the spin density plots, indicated in yellow ($\rho_{iso} = 0.01$ e$^-$/Å^3).

different sizes: Zr$_{16}$O$_{32}$, Zr$_{40}$O$_{80}$, and Zr$_{80}$O$_{160}$. The work performed so far shows that more than the size what counts are the morphological aspects and the presence of low coordinated sites. In this respect, the smallest and largest particles considered, Zr$_{16}$O$_{32}$ and Zr$_{80}$O$_{160}$, are electronically similar and behave differently from the zirconia (101) surface, whereas the intermediate size Zr$_{40}$O$_{80}$ has a general behavior, which is reminiscent of that of the bare zirconia surface. We modeled adsorption of the two H atoms on next-neighbor Zr or O sites at the corners of the NPs as these sites are expected to be more reactive because of their low coordination. The dissociation of H_2 on these sites is largely exothermic, Table 1. The reaction energy of the hydrogenation step is −1.79, −1.80, and −1.62 eV, respectively, on Zr$_{80}$O$_{160}$, Zr$_{40}$O$_{80}$, and Zr$_{16}$O$_{32}$ NPs, Table 1. We have recently reported such high reactivity of nanostructured zirconia compared to extended flat and stepped zirconia surfaces (for a more detailed description of this process, the reader is referred to ref 20). Zr$_{80}$O$_{160}$ and Zr$_{16}$O$_{32}$ split the H_2 molecule through a homolytic mechanism, which implies the direct reduction of the oxide via formation of Zr^{3+} centers (Figure 1b,d) and adsorbed protons. The heterolytic dissociation is energetically unfavorable compared to the homolytic process. On the contrary, Zr$_{40}$O$_{80}$ splits H_2 heterolytically, as for the regular (101) surface, with no reduction of the oxide (Figure 1c). In this case, the homolytic process lies higher in energy. We attribute this difference to the different shape, and consequently to the different electronic structure, of the three NPs. In particular, the presence of low-lying Zr 4d states in the energy gap of Zr$_{80}$O$_{160}$ and Zr$_{16}$O$_{32}$, owing to the low coordinated Zr ions at corners and edges (Figure 2b,d), favors the reduction of Zr^{4+} to Zr^{3+}. By contrast, the energy gap of Zr$_{40}$O$_{80}$ (Figure 2c) does not exhibit such defective states, in analogy with the (101) surface (Figure 2a). The exothermicity of the hydrogenation on Zr$_{40}$O$_{80}$ comes from the special structural flexibility that enhances its reactivity rather than from electronic effects due to low coordination of the Zr ions.

The entropic terms also make the H_2 dissociation less exergonic, resulting in Gibbs free energies of −1.19, −1.33, and −1.01 eV on Zr$_{80}$O$_{160}$, Zr$_{40}$O$_{80}$, and Zr$_{16}$O$_{32}$, respectively. Note that these values are qualitatively different from those corresponding to the (101) surface, where the reaction has a positive ΔG, Table 1. In addition, the OH and ZrH stretching frequencies from both the homolytic and heterolytic mechanisms are significantly blue-shifted in the NPs (~3700 cm^{-1}) compared to those on the regular (101) surface (~3000 cm^{-1}). This can be attributed to longer OH and ZrH bonds in the

Table 1. Stretching Frequencies, ν_{X-H} (X = O and Zr), Preferred H_2 Dissociation Mechanism, Reaction DFT Energy, ΔE, and Reaction Gibbs Free Energy at 298 K and 1 bar, ΔG, for Steps I and II

		I—hydrogenation			II—dehydration	
support	ν_{X-H} (cm^{-1})	mechanism	ΔE_I (eV)	ΔG_I (eV)	ΔE_{II} (eV)	ΔG_{II} (eV)
ZrO_2 (101)	OH: 2931, ZrH: 1394	heterolytic	−0.06	+0.34	+3.55	+3.28
$Zr_{80}O_{160}$	OH: 3758, OH: 3755	homolytic	−1.79	−1.19	+2.03	+1.55
$Zr_{40}O_{80}$	OH: 3740, ZrH: 1589	heterolytic	−1.80	−1.33	+3.08	+2.74
$Zr_{16}O_{32}$	OH: 3830, OH: 3785	homolytic	−1.62	−1.01	+2.04	+1.56
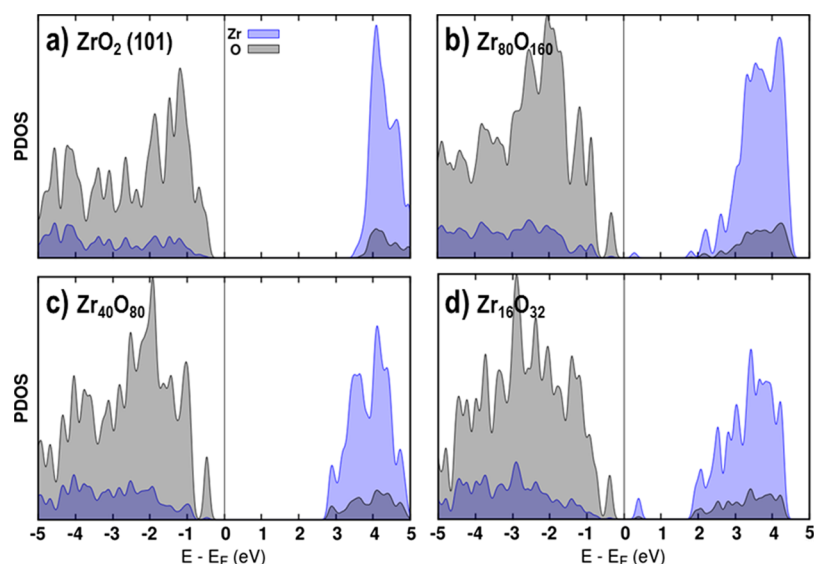
Figure 2. Projected density of states (PDOS) of (a) the ZrO_2 (101) surface, (b) $Zr_{80}O_{160}$, (c) $Zr_{40}O_{80}$, and (d) $Zr_{16}O_{32}$. The zero of energy corresponds to the top of the valence states. The PDOS of O atoms is indicated in gray and that of Zr atoms is indicated in blue.

Table 2. Temperature in K at Which ΔG_I and $\Delta G_{II} < 0$ (Spontaneous Process) at $P = 1$ bar and $P = 10^{-12}$ bar

	I—hydrogenation		II—dehydration	
support	$P(H_2) = 1$ bar	$P(H_2) = 10^{-12}$ bar	$P(H_2O) = 1$ bar	$P(H_2O) = 10^{-12}$ bar
ZrO_2 (101)	<70	<25	>1525	>790
$Zr_{80}O_{160}$	<930	<410	>920	>450
$Zr_{40}O_{80}$	<995	<445	>1350	>680
$Zr_{16}O_{32}$	<840	<365	>920	>450

(101) surface due to an electrostatic attraction between the H^+ and H^- ions, Figure 1a.

The second step implies the desorption of a water molecule from the hydrogenated surface with the subsequent formation of an O vacancy (dehydration). This process involves the diffusion of a H atom on the surface and its binding to an OH group with the formation of an O_sH_2 unit. In the (101) surface, this step has an energy cost of 3.55 eV. In this case, a slightly lower Gibbs free energy is obtained because the entropy of the H_2O gas favors desorption (3.28 eV at 298 K and 1 bar, Table 1), but the process remains significantly endergonic. In the NPs, ΔG_{II} is also endergonic but considerably smaller, about 1.5 eV for both $Zr_{80}O_{160}$ and $Zr_{16}O_{32}$ (Table 1); on the contrary, the cost remains high on $Zr_{40}O_{80}$ (ΔE_{II} = 3.08 eV and ΔG_{II} = 2.74 eV) where a heterolytic dissociation of hydrogen has occurred, Table 1. The reduction of the energy cost comes from the stabilization of the O vacancies in the NPs. In the (101) surface, the creation of a vacancy costs around 6 eV with respect to the formation of $1/2O_2$,[12] whereas in $Zr_{80}O_{160}$, $Zr_{40}O_{80}$, and $Zr_{16}O_{32}$, the cost is 2.77, 3.82, and 2.96 eV, respectively.[7,8] It is important to note that the results show that

the creation of an O vacancy in ZrO_2 by desorption of H_2O has a lower cost than via desorption of oxygen and formation of $1/2O_2$. This holds true for both NPs and surfaces.

From the thermodynamic data, we have calculated the reaction conditions at which the Gibbs free energy becomes negative (exergonic); hence, the process becomes thermodynamically spontaneous. For that, we have considered the entropy of the H_2 and H_2O gases at different temperatures between 50 and 1600 K and for pressures of 1 bar (ambient) and 10^{-12} bar (ultrahigh vacuum, UHV) according to eqs 5−67. Thus, a trend ΔG versus T is constructed for each pressure and reaction step. The temperatures at which the condition $\Delta G = 0$ is satisfied are reported in Table 2. For the hydrogenation process, H_2 dissociates spontaneously on the (101) surface at 1 bar and below 70 K because of the low reactivity of the extended zirconia toward H_2 dissociation (for higher temperatures, H_2 desorption dominates). On the contrary, the NPs can be hydrogenated at ambient pressure in a wide range of temperatures, up to 800−900 K (Table 2) because of the high reactivity toward H_2 (exergonic adsorption free energies of −1/−1.3 eV, Table 1). Above this temperature range, the entropy
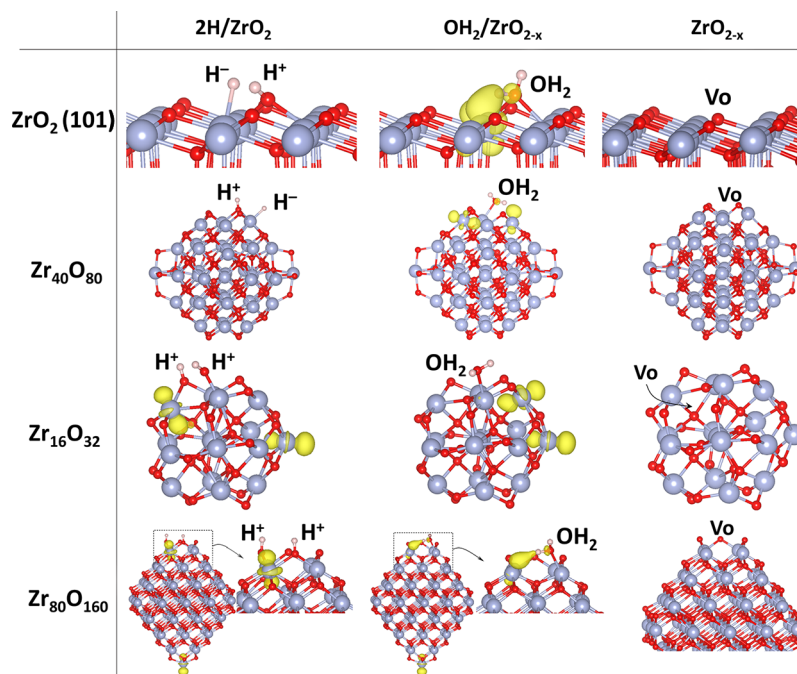
Figure 3. Structures of the energy minimums for the dehydration process from the heterolytically hydrogenated ZrO_2 (101) surface and $Zr_{40}O_{80}$ and the homolytically hydrogenated $Zr_{16}O_{32}$ and $Zr_{80}O_{160}$ NPs. Zr: blue atoms; O: red atoms; and H: white atoms. The spin density is indicated in yellow (ρ_{iso} = 0.01 e$^-$/Å^3).

contribution of H_2 prevents its adsorption to the surface and favors desorption.

The desorption of water from the heterolytically dissociated 2H/ZrO_2 (101) surface at ambient pressure requires temperatures above 1500 K because of the high endergonic character of the process (ΔG_{II} = +3.28 eV) or above 800 K when the partial pressure of water decreases to UHV conditions (10^{-12} bar). As in the initial hydrogenation step, NPs can undergo dehydration at milder conditions compared to the regular surface. In particular, water can start desorbing from the surface, creating an O vacancy at temperatures above 450 K, a temperature at which several catalytic processes involving oxides start to occur.[6] In summary, NPs of zirconia can dissociate hydrogen and desorb water at milder reaction conditions compared to the extended surface, changing completely the landscape for the chemistry of these systems. In the special case of zirconia, this leads a nonreducible oxide to become reducible when prepared in a nanostructured form.

3.2. Kinetic Aspects (Energy Barriers). In this section, we investigate the complete reaction energy path, from the adsorption of H_2 to the formation and desorption of H_2O, including the reaction barriers. This can be divided into two steps, as mentioned above. The first step involves the physisorption of H_2 followed by its dissociation (homo- or heterolytic); the second step is the diffusion of hydrogen on the surface and the formation of an OH_2 surface complex; and the last step is related to the desorption of H_2O from the surface, leaving behind an O vacancy.

First, on the ZrO_2 (101) surface, the H_2 molecule is physisorbed with an energy of −0.11 eV; it dissociates heterolytically into H$^+$ and H$^-$ species through a small energy barrier of 0.28 eV and a small binding of −0.06 eV (see above). A similar barrier for the heterolytic dissociation was recently published by our group (0.24 eV[35]). Experimentally, such a barrier has been estimated to be around 0.4 eV.[50] To induce

water desorption, the H$^-$ ion must diffuse into the O−H$^+$ group and form a O_sH_2 unit (this can also be seen as a H_2O molecule adsorbed on a surface O vacancy). This process forces the system to become reduced. In fact, when the two H atoms are bound to the same oxygen (O_sH_2 surface complex), the excess of charge is localized on two Zr^{3+} centers in a triplet state (Figure 3); it is the same configuration obtained when two H atoms are adsorbed on two different oxygen sites, resulting in a homolytic cleavage of the H−H bond (excited state). This state is energetically highly unfavorable, and in fact, this process is noncompetitive with respect to H_2 desorption. Still, it is a necessary step for water desorption. When the O_sH_2 surface complex is formed, two electrons are transferred to two Zr ions (Zr^{3+}). This is different from the case of O-deficient zirconia (O vacancy) where electrons localize in the vacancy and give rise to a singlet ground state (Figure 3) because of the morphological change in the structure connected to the O removal. The formation of the O_sH_2 complex on the regular surface by H diffusion is thus highly endothermic, ΔE = +2.79 eV, and the barrier is obviously even higher, 2.93 eV. A lower barrier, 2.55 eV, has been reported in a previous study by our group using a slightly different computational approach.[35] Once the O_sH_2 surface complex is formed, it desorbs with an energy cost of 0.72 eV. Therefore, the highest barrier in the entire process is the diffusion of a H atom to form a O_sH_2 precursor state of the desorbing water molecule; neglecting prefactors, this is the rate-determining step with a very high energy barrier, close to 3 eV. This process will hardly occur on the bare zirconia surface as H_2 desorption is clearly preferred.

Now, we consider zirconia NPs where lower energy barriers are expected for the formation and desorption of the H_2O molecule. In Figure 4, the reaction energy profiles for the dehydration step from the hydrogenated NPs are compared with those from the (101) surface. We did not study in detail the physisorption and the barrier for dissociation of the H_2
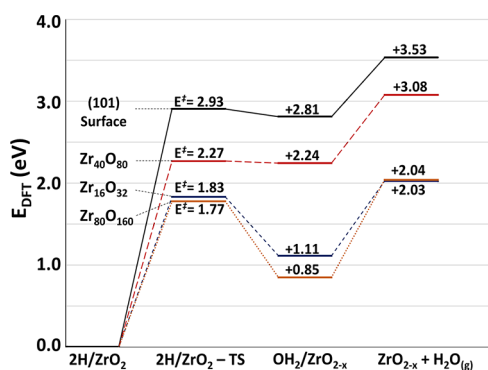
Figure 4. Reaction energy profiles for the dehydration step of the hydrogenated $2H/ZrO_2$ NPs (dashed line) and the extended $2H/ZrO_2$ (101) surface (solid line).

molecule, assuming that these values are not going to be very different from the regular (101) surface (−0.11 and 0.28 eV, respectively). In general, considering that the adsorption energies of H_2 on the ZrO_2 NPs are of −1.6/−1.8 eV, Table 1, the small changes in H_2 physisorption and barriers for dissociation when the process is considered on zirconia NPs are not expected to play a role in the whole process. The energy profiles reported are thus starting from the hydrogenated surface.

On the NPs, one H atom diffuses from the OH or the ZrH groups to another OH group, which can be two-coordinated or even single-coordinated, as in $Zr_{16}O_{32}$ (Figure 1d). Also in this case, the overall NP−O_sH_2 complex assumes a triplet ground state with two localized Zr^{3+} sites, Figure 3. Interestingly, the energy barrier decreases from 2.93 eV on the extended surface to 1.77 eV in $Zr_{80}O_{160}$ NPs and to 1.83 eV in $Zr_{16}O_{32}$ NPs. This is a very significant reduction of more than 1 eV. It has the important consequence that H diffusion competes with H_2 desorption, differently from the bare surface. The subsequent desorption of H_2O has a cost of 0.85 eV in $Zr_{80}O_{160}$ and 1.11 eV in $Zr_{16}O_{32}$. Thus, also on the NPs, the highest barrier is not associated with the water desorption but rather with the hydrogen diffusion and with the formation of the precursor state. Despite the large decrease in the barrier, this does not reach the low value found for TiO_2, a typical reducible oxide, where the barrier for a similar process has been estimated to be around 0.3 eV.[33]

Things are partly different for the $Zr_{40}O_{80}$ NP. We have seen above that on this NP the thermodynamics for the reduction reaction is similar to that of the (101) surface because of a similar electronic structure with the absence of defective states in the band gap (Figure 2c). Accordingly, the reaction energy path for the dehydration of $2H/Zr_{40}O_{80}$ has some resemblance with that of the extended surface; the energy cost to form the O_sH_2 precursor is lower (2.24 eV) because of the higher structural flexibility of the nanostructure, and so is the barrier (2.27 eV). From this state, water desorbs to the gas phase with a cost of 0.84 eV. Thus, also in this case, the highest barrier is associated with hydrogen diffusion. The barrier is considerably lower than that on the regular surface (2.27 vs 2.93 eV) but still much larger than those on the other two zirconia NPs considered (about 1.8 eV) where the mechanism of H_2 dissociation is different.

These results show the positive effect of nanostructuring on the reducibility of zirconia by water removal. The special fluxionality of the NPs contributes to lowering not only the

energy costs but also the energy barriers involved in the process, thanks to a larger atomic relaxation around the created O vacancy. This structural flexibility is much smaller or even absent in bulk ZrO_2 and ZrO_2 surface. However, comparing the different behaviors of $Zr_{80}O_{160}$ and $Zr_{16}O_{32}$ NPs with that of $Zr_{40}O_{80}$ NPs, one can conclude that the key factor is the presence of low-lying acceptor states introduced in the electronic structure by low coordinated Zr sites in corners and edges, which strongly depends on the morphology of the NP.

There is a final aspect that needs to be discussed and that, once more, shows a different behavior for the extended zirconia surface compared to that of the NPs. We are referring to the process for H diffusion on the hydrogenated surface. In the initial state, the two H atoms remain adsorbed on vicinal sites (e.g., a Zr and an O ion, in the case of heterolytic splitting). On the ZrO_2 (101) surface, the displacement of H^+ and H^- ions to more distant O and Zr sites has an energy cost of 0.64 and 0.73 eV, respectively, and it implies to overcome a barrier of 1.50 (H^+) and 1.42 (H^-) eV, Table 3. The fact that separating the

Table 3. Diffusion Energy, ΔE_{diff}, and Energy Barrier, $\Delta E^{\ddagger}$, for the Diffusion of a H Atom into Adsorption Sites Distant from the OH^+ Precursor for the H_2O Formation

support		ΔE_{diff} (eV)	$\Delta E^{\ddagger}$ (eV)
ZrO_2 (101)	OH^+ to O'	0.64	1.50
	ZrH^- to Zr'	0.73	1.42
$Zr_{80}O_{160}$	$O_{2c}H^+$ to O_{3c}	0.69	1.73
$Zr_{40}O_{80}$	$O_{2c}H^+$ to O_{3c}	0.84	1.58
	ZrH^- to Zr_{facet}	0.24	2.15
$Zr_{16}O_{32}$	$O_{2c}H^+$ to O_{2c}	0.06	1.72
	$O_{2c}H^+$ to O_{3c}	0.50	1.54

two species has a relatively high energy cost is due to their opposite charges. The barrier is sufficiently high that, at low H_2 pressure, molecular desorption rather than diffusion is expected. This means that the formation of the O_sH_2 surface complex is a rather unlikely event on the bare (101) ZrO_2 surface.

Things are different for the NPs. In $Zr_{80}O_{160}$ and $Zr_{16}O_{32}$, the diffusion of one of the H^+ species into an O site on one facet costs 0.69 and 0.50 eV, respectively, depending on the coordination number of the O atom. Despite the fact that two positive charges are separated, the proton goes from an O_{2c} site in the corner to a less reactive O_{3c} in the facet, with a concomitant decrease in stability. On $Zr_{16}O_{32}$, where the diffusion involves two O_{2c} corner sites, the cost is 0.06 eV only. For the same reason, in $Zr_{40}O_{80}$, the diffusion costs 0.84 and 0.24 eV for H^+ and H^- ions moving to different O and Zr sites in the facet, respectively. The barrier for diffusion on the NPs is rather high, on the order of 1.5−2 eV, not very different from what was calculated for the bare (101) surface. However, on the NPs, this energy barrier is comparable to that required to form the O_sH_2 surface complex, suggesting that here the hydrogen diffusion and water desorption become competitive processes.

4. CONCLUSIONS

We have performed, by means of DFT-based calculations with the PBE + U exchange−correlation functional and D2' dispersion, a comparative study of the reduction reaction $ZrO_2 + H_2 \rightarrow ZrO_{2-x} + H_2O$ in nanostructured zirconia and in the regular (101) surface. This has been separated into two steps: hydrogenation of the surface (step I) and subsequent

removal of a water molecule with the formation of an O vacancy (step II).

Because of the low reducibility of ZrO_2, the reduction process of the extended (101) surface is unfavorable, with energies $\Delta E_I = -0.06$ eV ($\Delta G_I = 0.34$ eV) and $\Delta E_{II} = 3.55$ eV ($\Delta G_{II} = 3.28$ eV). Zirconia NPs are more reactive, resulting in significantly lower reaction energies, $\Delta E_I = -1.6$ to -1.8 eV ($\Delta G_I = -1$ to -1.2 eV) and $\Delta E_{II} = 2-3$ eV ($\Delta G_{II} = 1.5-2.7$ eV), because of their special structural flexibility and electronic structure. In a real system, there will be a random distribution of Zr^{3+} ions on the surface of the NPs. The disorder introduced by this distribution of sites will provide a configurational entropy contribution that is going to provide an extra stabilization for the reduced NPs compared to the bare surface.

However, the mechanism for H_2 splitting is determined by the electronic structure. On the (101) surface, H_2 is dissociated heterolytically (formation of OH^+ and ZrH^- species). On $Zr_{80}O_{160}$ and $Zr_{16}O_{32}$ NPs, the presence of low-lying Zr 4d acceptor states from low coordinated Zr ions at corners and edges favors the homolytic H_2 splitting, which implies the direct reduction of the oxide (formation of two OH^+ species and two Zr^{3+} centers). By contrast, such states are not present in $Zr_{40}O_{80}$ where the H_2 molecule dissociates heterolytically as on the (101) surface. This demonstrates that not only the dimensions of the NPs count but also their shape and surface morphology.

From the thermodynamic data, we conclude that the hydrogenation reaction at ambient pressure (1 bar) can be performed at any temperature up to 900 K on the NPs, whereas on the (101) surface, it is possible only below 70 K (the competitive mechanism is H_2 desorption).

For the dehydration step, the energy barrier to form a H_2O molecule on the hydrogenated surface decreases from 2.93 eV on the (101) surface to 2.27 in $Zr_{40}O_{80}$ (which is more "bulklike") and to 1.77 and 1.83 eV in $Zr_{80}O_{160}$ and $Zr_{16}O_{32}$, respectively. As a consequence, under UHV conditions, the dehydration of the hydrogenated (101) surface requires temperatures above 800 K, whereas on the NPs, it is possible above 450 K, a typical reaction temperature in many catalytic processes. The results presented refer to the cases where only one H_2 molecule has been adsorbed on the surface of the zirconia NPs. However, under working conditions, the particle will be fully hydrogenated, and coverage effects will play a role. In particular, we expect lower barriers for hydrogen migration to form the O_sH_2 surface complex; also, the presence of excess electrons due to the high hydrogen coverage can facilitate water desorption. In general, this work shows the importance of nanostructuring for the chemistry of oxides as this completely modifies the oxide reducibility.

AUTHOR INFORMATION

Corresponding Author
*E-mail: Gianfranco.pacchioni@unimib.it (G.P.).

ORCID
Francesc Illas: 0000-0003-2104-6123
Gianfranco Pacchioni: 0000-0002-4749-0751

Notes
The authors declare no competing financial interest.

ACKNOWLEDGMENTS

REFERENCES

(1) Wang, J.; You, Z.; Zhang, Q.; Deng, W.; Wang, Y. Synthesis of Lower Olefins by Hydrogenation of Carbon Dioxide over Supported Iron Catalysts. *Catal. Today* **2013**, *215*, 186−193.

(2) Rhodes, M. D.; Bell, A. T. The Effects of Zirconia Morphology on Methanol Synthesis from CO and H_2 over Cu/ZrO$_2$ Catalysts: Part I. Steady-state Studies. *J. Catal.* **2005**, *233*, 198−209.

(3) Nakano, Y.; Yamaguchi, T.; Tanabe, K. Hydrogenation of Conjugated Dienes over ZrO$_2$ by H_2 and Cyclohexadiene. *J. Catal.* **1983**, *80*, 307−314.

(4) Sun, C.; Stimming, U. Recent Anode Advances in Solid Oxide Fuel Cells. *J. Power Sources* **2007**, *171*, 247−260.

(5) Pacchioni, G. Ketonization of Carboxylic Acids in Biomass Conversion over TiO$_2$ and ZrO$_2$ Surfaces: A DFT Perspective. *ACS Catal.* **2014**, *4*, 2874−2888.

(6) Pham, T. N.; Sooknoi, T.; Crossley, S. P.; Resasco, D. E. Ketonization of carboxylic acids: mechanisms, catalysts, and implications for biomass conversion. *ACS Catal.* **2013**, *3*, 2456−2473.

(7) Puigdollers, A. R.; Illas, F.; Pacchioni, G. Structure and Properties of Zirconia Nanoparticles from Density Functional Theory Calculations. *J. Phys. Chem. C* **2016**, *120*, 4392−4402.

(8) Puigdollers, A. R.; Illas, F.; Pacchioni, G. ZrO$_2$ Nanoparticles: A Density Functional Theory Study of Structure, Properties and Reactivity. *Rend. Fis. Acc. Lincei* **2017**, *28*, 19−27.

(9) Chrétien, S.; Metiu, H. Acid−Base Interaction and Its Role in Alkane Dissociative Chemisorption on Oxide Surfaces. *J. Phys. Chem. C* **2014**, *118*, 27336−27342.

(10) Korhonen, S. T.; Calatayud, M.; Krause, A. O. I. Stability of Hydroxylated ($\bar{1}$11) and ($\bar{1}$01) Surfaces of Monoclinic Zirconia: A Combined Study by DFT and Infrared Spectroscopy. *J. Phys. Chem. C* **2008**, *112*, 6469−6476.

(11) Yamaguchi, T. Application of ZrO2 as A Catalyst and A Catalyst Support. *Catal. Today* **1994**, *20*, 199−217.

(12) Ganduglia-Pirovano, M. V.; Hofmann, A.; Sauer, J. Oxygen Vacancies in Transition Metal and Rare Earth Oxides: Current State of Understanding and Remaining Challenges. *Surf. Sci. Rep.* **2007**, *62*, 219−270.

(13) Migani, A.; Vayssilov, G. N.; Bromley, S. T.; Illas, F.; Neyman, K. M. Greatly facilitated oxygen vacancy formation in ceria nanocrystallites. *Chem. Commun.* **2010**, *46*, 5936−5938.

(14) Melchionna, M.; Fornasiero, P. The role of ceria-based nanostructured materials in energy applications. *Mater. Today* **2014**, *17*, 349−357.

(15) Alivisatos, A. P. Semiconductor Clusters, Nanocrystals, and Quantum Dots. *Science* **1996**, *271*, 933−937.

(16) Dosch, H. Some General Aspects of Confinement in Nanomaterials. *Appl. Surf. Sci.* **2001**, *182*, 192−195.

(17) Majetich, S. A.; Jin, Y. Magnetization Directions of Individual Nanoparticles. *Science* **1999**, *284*, 470−473.

(18) Leconte, J.; Markovits, A.; Skalli, M. K.; Minot, C.; Belmajdoub, A. Periodic Ab Initio Study of the Hydrogenated Rutile TiO$_2$(110) Surface. *Surf. Sci.* **2002**, *497*, 194−204.

(19) Calatayud, M.; Markovits, A.; Minot, C. Electron-count Control on Adsorption upon Reducible and Irreducible Clean Metal-oxide Surfaces. *Catal. Today* **2004**, *89*, 269−278.

(20) García-Melchor, M.; López, N. Homolytic Products from Heterolytic Paths in H_2 Dissociation on Metal Oxides: The Example of CeO_2. *J. Phys. Chem. C* **2014**, *118*, 10921−10926.

(21) Puigdollers, A. R.; Tosoni, S.; PAcchioni, G. Turning a Nonreducible into a Reducible Oxide via Nanostructuring: Opposite Behavior of Bulk ZrO_2 and ZrO_2 Nanoparticles Toward H_2 Adsorption. *J. Phys. Chem. C* **2016**, *120*, 15329−15337.

(22) Pham, T. N.; Sooknoi, T.; Crossley, S. P.; Resasco, D. E. Ketonization of Carboxylic Acids: Mechanisms, Catalysts, and Implications for Biomass Conversion. *ACS Catal.* **2013**, *3*, 2456−2473.

(23) Barteau, M. A. Organic Reactions at Well-Defined Oxide Surfaces. *Chem. Rev.* **1996**, *96*, 1413−1430.

(24) Hoang, D. L.; Lieske, H. Effect of Hydrogen Treatments on ZrO_2 and Pt/ZrO_2 Catalysts. *Catal. Lett.* **1994**, *27*, 33−42.

(25) Sinhamahapatra, A.; Jeon, J.-P.; Kang, J.; Han, B.; Yu, J.-S. Oxygen-Deficient Zirconia ($ZrO_{2−x}$): A New Material for Solar Light Absorption. *Sci. Rep.* **2016**, *6*, 27218.

(26) Rahman, M. A.; Rout, S.; Thomas, J. P.; McGillivray, D.; Leung, K. T. Defect-rich Dopant-Free ZrO_2 Nanostructures with Superior Dilute Ferromagnetic Semiconductor Properties. *J. Am. Chem. Soc.* **2016**, *138*, 11896−11906.

(27) Chen, H.-Y. T.; Tosoni, S.; Pacchioni, G. Adsorption of Ruthenium Atoms and Clusters on Anatase TiO_2 and Tetragonal ZrO_2 (101) Surfaces: A Comparative DFT Study. *J. Phys. Chem. C* **2015**, *119*, 10856−10868.

(28) Pacchioni, G.; Pescarmona, P. Structure and Stability of Oxygen Vacancies on Sub-Surface, Terraces, and Low-Coordinated Surface Sites of MgO: An Ab Initio Study. *Surf. Sci.* **1998**, *412*, 657−671.

(29) Pacchioni, G.; Freund, H. Electron Transfer at Oxide Surfaces. The MgO Paradigm: From Defects to Ultrathin Films. *Chem. Rev.* **2013**, *113*, 4035−4072.

(30) Vayssilov, G. N.; Lykhach, Y.; Migani, A.; Staudt, T.; Petrova, G. P.; Tsud, N.; Skála, T.; Bruix, A.; Illas, F.; Prince, K. C.; Matolín, V.; Neyman, K. M.; Libuda, J. Support Nanostructure Boosts Oxygen Transfer to Catalytically Active Platinum Nanoparticles. *Nat. Mater.* **2011**, *10*, 310−315.

(31) Vayssilov, G. N.; Gates, B. C.; Rösch, N. Oxidation of Supported Rhodium Clusters by Support Hydroxy Groups. *Angew. Chem., Int. Ed.* **2003**, *42*, 1391−1394.

(32) Mager-Maury, C.; Chizallet, C.; Sautet, P.; Raybaud, P. Platinum Nanoclusters Stabilized on γ-Alumina by Chlorine Used as A Capping Surface Ligand: A Density Functional Theory Study. *ACS Catal.* **2012**, *2*, 1346−1357.

(33) Chen, H.-Y. T.; Tosoni, S.; Pacchioni, G. Hydrogen Adsorption, Dissociation, and Spillover on Ru_{10} Clusters Supported on Anatase TiO_2 and Tetragonal ZrO_2 (101) Surfaces. *ACS Catal.* **2015**, *5*, 5486−5495.

(34) Hofmann, A.; Clark, S. J.; Oppel, M.; Hahndorf, I. Hydrogen Adsorption on the Tetragonal ZrO2 (101) Surface: A Theoretical Study of an Important Catalytic Reactant. *Phys. Chem. Chem. Phys.* **2002**, *4*, 3500−3508.

(35) Tosoni, S.; Pacchioni, G. Acetic Acid Ketonization on Tetragonal Zirconia: Role of Surface Reduction. *J. Catal.* **2016**, *344*, 465−473.

(36) Ishikawa, H.; Kondo, J. N.; Domen, K. Hydrogen Adsorption on Ru/ZrO_2 Studied by FT-IR. *J. Phys. Chem. B* **1999**, *103*, 3229−3234.

(37) Puigdollers, A. R.; Illas, F.; Pacchioni, G. Effect of nanostructuring on the reactivity of zirconia: A DFT+U study of Au atom adsorption. *J. Phys. Chem. C* **2016**, *120*, 17604−17612.

(38) Kresse, G.; Furthmüller, J. Efficiency of ab-Initio Total Energy Calculations for Metals and Semiconductors Using a Plane-Wave Basis Set. *Comput. Mater. Sci.* **1996**, *6*, 15−50.

(39) Kresse, G.; Furthmüller, J. Efficient Iterative Schemes for Ab Initio Total-Energy Calculations Using a Plane-Wave Basis Set. *Phys. Rev. B: Condens. Matter Mater. Phys.* **1996**, *54*, 11169−11186.

(40) Perdew, J. P.; Burke, K.; Ernzerhof, M. Generalized Gradient Approximation Made Simple. *Phys. Rev. Lett.* **1996**, *77*, 3865−3868.

(41) Anisimov, V. I.; Zaanen, J.; Andersen, O. K. Band Theory and Mott Insulators: Hubbard U instead of Stoner I. *Phys. Rev. B: Condens. Matter Mater. Phys.* **1991**, *44*, 943−954.

(42) Dudarev, S. L.; Botton, G. A.; Savrasov, S. Y.; Humphreys, C. J.; Sutton, A. P. Electron-Energy-Loss Spectra and the Structural Stability of Nickel Oxide: An LSDA+U Study. *Phys. Rev. B: Condens. Matter Mater. Phys.* **1998**, *57*, 1505−1509.

(43) Teufer, G. The Crystal Structure of Tetragonal ZrO_2. *Acta Crystallogr.* **1962**, *15*, 1187.

(44) French, R. H.; Glass, S. J.; Ohuchi, F. S.; Xu, Y.-N.; Ching, W. Y. Experimental and Theoretical Determination of the Electronic Structure and Optical Properties of Three Phases of ZrO_2. *Phys. Rev. B: Condens. Matter Mater. Phys.* **1994**, *49*, 5133−5142.

(45) Tosoni, S.; Sauer, J. Accurate Quantum Chemical Energies for the Interaction of Hydrocarbons with Oxide Surfaces: CH_4/MgO-(001). *Phys. Chem. Chem. Phys.* **2010**, *12*, 14330−14340.

(46) Grimme, S. Semiempirical GGA-Type Density Functional Constructed with a Long-Range Dispersion Correction. *J. Comput. Chem.* **2006**, *27*, 1787−1799.

(47) Tosoni, S.; Sauer, J. Accurate quantum chemical energies for the interaction of hydrocarbons with oxide surfaces: $CH_4/MgO(001)$. *Phys. Chem. Chem. Phys.* **2010**, *12*, 14330−14340.

(48) *CRC Handbook of Chemistry and Physics*, 89th ed.; Lide, D. R., Ed.; CRC Press/Taylor and Francis: Boca Raton, FL, 2008.

(49) Henkelman, G.; Uberuaga, B. P.; Jónsson, H. A Climbing Image Nudged Elastic Band Method for Finding Saddle Points and Minimum Energy Paths. *J. Chem. Phys.* **2000**, *113*, 9901−9904.

(50) Kondo, J.; Sakata, Y.; Domen, K.; Maruya, K.-i.; Onishi, T. Infrared Study of Hydrogen Adsorbed on ZrO_2. *J. Chem. Soc., Faraday Trans.* **1990**, *86*, 397−401.